Inorganic Chemistry

Article

pubs.acs.org/IC

The Solid Solution Series $(GeTe)_x(LiSbTe_2)_2$ ($1 \leq x \leq 11$) and the Thermoelectric Properties of $(GeTe)_{11}(LiSbTe_2)_2$

Thorsten Schröder,[†] Stefan Schwarzmüller,[†] Christian Stiewe,[‡] Johannes de Boor,[‡] Markus Hölzel,[§] and Oliver Oeckler*[,∥]

[†]LMU Munich, Department of Chemistry, Butenandtstr. 5-13 (D), 81377 Munich, Germany

[‡]German Aerospace Center, Linder Höhe, 51147 Cologne, Germany

[§]Forschungsneutronenquelle Heinz Maier-Leibnitz (FRM II), TUM, Lichtenbergstr. 1, 85747 Garching, Germany

[∥]Leipzig University, IMKM, Scharnhorststr. 20, 04275 Leipzig, Germany

Supporting Information

ABSTRACT: Exchanging one Ge^{2+} with two Li^+ per formula unit in $(GeTe)_n(Sb_2Te_3)$ (n = 1, 2, 3, ...) eliminates cation vacancies, because it leads to an equal number of cations and anions. This substitution results in the solid solution $(GeTe)_x(LiSbTe_2)_2$ (with $x = n - 1$, but n not necessarily an integer). For $x < 6$, these stable compounds crystallize in a rock-salt-type structure with random cation disorder. Neutron data show that a small fraction of Ge occupies tetrahedral voids for $x = 2$ and 3. For $x > 6$, $(GeTe)_x(LiSbTe_2)_2$ forms a GeTe-type structure that shows a phase transition to a cubic high-temperature phase at ca. 280 °C. The thermoelectric properties of $(GeTe)_{11}(LiSbTe_2)_2$ have been investigated and show that this compound is a promising thermoelectric material with a ZT value of 1.0 at 450 °C. The high ZT value of the thermodynamically stable compound is caused by a low phononic contribution to the thermal conductivity; probably, Li acts as a "pseudo-vacancy".

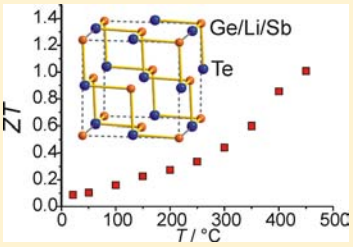

1. INTRODUCTION

Compounds with the composition $(GeTe)_n(Sb_2Te_3)$ (so-called GST materials) represent the most important class of phase-change materials (PCMs) for both optical and nonvolatile electrical data storage. They are used in rewritable DVDs and Blu-ray discs as well as in random access memory devices.[1−4] At ambient conditions, the thermodynamically stable state of these compounds corresponds to trigonal long-periodically ordered layered structures, in which slightly distorted rock-salt-type slabs are separated by van der Waals gaps with partially covalent Te−Te interactions.[5−7] For GeTe contents $n \geq 3$, a rock-salt-type high-temperature (HT) phase exists.[8] In the trigonal modification, Ge and Sb are disordered on the cation positions, which, in the cubic HT phase, are shared by Ge, Sb, and a fraction of $1/(n + 3)$ cation vacancies. Thus, the HT phase corresponds to the metastable crystalline phase in thin PCM films.[9,10] The disordered vacancies are a consequence of the fact that the charge balanced state contains fewer cations than anions. In PCMs, the origin of vacancies and their impact on properties have also attracted much attention recently.[11−14] In both trigonal and cubic phases, Te occupies the anion positions. Quenching the cubic HT phase leads to metastable (pseudo)-cubic compounds that are characterized by intersecting cation vacancy layers with limited lateral extension perpendicular to the cubic ⟨111⟩ directions. They are, however, not equidistantly spaced. The distorted NaCl-type building blocks between these planar defects form a "parquet-like" nanostructure. As the nanostructure depends on the defect concentration and diffusion, it is strongly influenced by the GeTe content n and the thermal treatment. For n = 12 and 19, these metastable compounds have remarkable thermoelectric properties and reach ZT values of ∼1.3 at 450 °C.[8,15] The dimensionless figure of merit $ZT = S^2T/\kappa\rho$ (Seebeck coefficient S, electrical resistivity ρ, thermal conductivity κ) is a measure of the efficiency of thermoelectric materials, which are an intriguing research subject since they can be used to reversibly interconvert electrical and thermal energy.[16−19] However, the high ZT values of GST materials are observed at temperatures where dynamical diffusion processes already set in and the stable trigonal modification is slowly formed. Therefore, the application potential of metastable GST as a thermoelectric material is limited up to 350 °C, where the maximum ZT value amounts to ∼0.7.

The instability of the (pseudo)cubic phases is probably due their high concentration of vacancies that involves "incomplete" coordination spheres and a large energy gain when ordered structures are formed. Therefore, they may be stabilized as quaternary compounds when the vacancy concentration is reduced, for example, by replacing Ge^{2+} by twice the amount of monovalent cations. This brings the cation/anion ratio closer to 1 and should increase the temperature range in which the materials can be applied. The use of Li^+ as a "pseudo-vacancy" may ensure a large mass difference between the atoms involved, which disturbs vibrational modes and hence lowers the phononic part of the thermal conductivity. Therefore, the

Received: June 18, 2013
Published: September 16, 2013

   dx.doi.org/10.1021/ic401516m | Inorg. Chem. 2013, 52, 11288−11294

thermoelectric properties of such quaternary phases are expected to be comparable to those of metastable quenched GST materials, including those that are used as PCMs.[20] In a comparable manner, a few percent of vacancies in $AgSbTe_2$ are beneficial for the thermoelectric properties by lowering κ without affecting ρ.[21]

2. EXPERIMENTAL SECTION

Synthesis. Samples with the composition $(GeTe)_x(LiSbTe_2)_2$ (x = 0, 1, 2, 3, 6, and 11) were synthesized by heating stoichiometric mixtures (e.g., 1.0 g) of the pure elements (lithium 99.999%, Alfa Aesar; germanium 99.999%, Sigma-Aldrich; antimony 99.9999%, Smart Elements; tellurium 99.999%, Alfa Aesar) to 700 °C under an Ar atmosphere for 1 h. For high Li contents (x = 0, 1, 2, 3), graphite crucibles in sealed silica ampoules were used; for lower Li contents, graphitized silica glass ampoules proved to be sufficient. The ampoules containing the resulting melts were quenched to room temperature in water. To obtain the amounts required for neutron diffraction, several samples with the same composition were combined, finely ground, and annealed for 12 h at 550 °C and cooled to RT in 2 h to ensure homogeneity. For the thermoelectric characterization, three samples (1.5 g) of the composition $(GeTe)_{11}(LiSbTe_2)_2$ were prepared as described and subsequently fused together by combining the samples in a larger ampoule, melting them for 10 min at 700 °C, and subsequently annealing them at 550 °C for 48 h. All compounds are slightly sensitive to moisture and show a basic reaction when mixed with water.

Diffraction Methods. X-ray powder patterns were recorded on a Huber G670 Guinier camera equipped with a fixed imaging plate and integrated read-out system using Cu-Kα_1 radiation (Ge monochromator, λ = 1.54051 Å). Specimens were prepared by crushing the samples in a glovebox under an Ar atmosphere and fixing the powder between two Mylar foils on a flat sample holder using vacuum grease. Temperature-dependent powder diffraction was performed with a STOE Stadi P powder diffractometer equipped with an imaging-plate detector system using Mo-Kα_1 radiation (Ge monochromator, λ = 0.71093 Å) in a modified Debye–Scherrer geometry equipped with a graphite furnace. Powdered samples were filled into silica glass capillaries with a 0.3 mm diameter and sealed with vacuum grease under an argon atmosphere. The measurement was performed from room temperature (RT) to 600 °C with a heating rate of 10 K/min and from 600 °C back to RT with a cooling rate of 5 K/min (faster cooling is impossible with the setup used).

Neutron powder diffraction patterns were acquired on the SPODI diffractometer at the neutron source FRM II (Munich, Germany, λ = 1.5484 Å, detector array of 80 position-sensitive ^{3}He tubes with a 300 mm active height, fixed Soller collimators of 10′ horizontal divergence). The samples (~3.0 g) were filled in vanadium crucibles under an Ar atmosphere. The angular range of $0° < 2\theta < 160°$ was covered by stepwise positioning of the detector array to obtain a diffraction pattern of 0.05° step width (2°/40 steps).

The phase homogeneity was determined by pattern fitting (Rietveld method) of X-ray data; structure data were obtained by joint refinements of X-ray and neutron data using the program TOPAS (details are given in the Results and Discussion section).[22]

ICP-OES. The chemical composition of the samples used for neutron diffraction was determined by inductively coupled plasma optical emission spectroscopy using a Varian Vista RL CCD Simultaneous ICP-OES. The samples (ca. 5 mg) were dissolved in a mixture of 1 mL of conc. HNO_3, 0.5 mL of conc. HCl, and 0.1 mL of HF (40% solution) and subsequently heated for 30 min at 105 °C. Two characteristic emission lines for each element were determined twice per sample and used to calculate an average. For Li only, the characteristic emission line at 670.783 nm was used. Although the samples were weighed with an accuracy of 0.0001 mg, the sum of the weight fractions of Li, Ge, Sb, and Te adds up to ~93%. As no other heavy elements are present, this can be attributed to hydrolysis effects. As there are no volatile products, the element ratios remain reliable. The experimental values (cf. Table S1 in the Supporting Information) are in excellent agreement with the ones corresponding to the starting mixture, which indicates that no significant amount of Li was lost by reaction with graphite crucibles.

Thermoelectric Characterization. The Seebeck coefficient (S) and electrical resistivity (ρ) of $(GeTe)_{11}(LiSbTe_2)_2$ were measured up to 450 °C under He using an in-house-built (DLR, Cologne, Germany) setup and commercial facilities for the determination of the thermal conductivity. The electrical resistance R was measured with an in-line four-point-probe setup made of tungsten carbide to avoid cable and contact resistances affecting the measurement and by using an ac method with a frequency of 7 Hz in order to reduce Peltier influences. The electrical resistivity follows as $\rho = (1/G_F)\cdot R$ (with the correction factor G_F taking into account the cross section and thickness of the sample and the distance between the probe tips). Seebeck coefficients were measured by establishing a small temperature gradient across the sample while the sample's environment temperature was changed and stabilized for each temperature step. Type-N thermocouples attached directly to the sample's surface were used for both the Seebeck voltage pickup and the temperature measurement.[23,24] The relative errors of $\rho(T)$ and $S(T)$ are 5%, respectively. The thermal conductivity κ was calculated with $\kappa = D_{th}\cdot\rho_m\cdot C_p$ from measurements of the thermal diffusivity D_{th} (determined using a laser-flash apparatus, LFA 427, Netzsch GmbH & Co., Germany), the mass density ρ_m (determined using a Mohr's balance), and the heat capacity C_p (determined using a differential scanning calorimeter, DSC 404, Netzsch GmbH & Co., Germany). A Lorenz number of 1.44×10^{-8} W Ω K^{-2} was used for calculating the electronic part of κ. The relative error of κ is ~8%, resulting from 3% for the D_{th} and 5% for the C_p.

3. RESULTS AND DISCUSSION

Crystal Structure Derived from X-ray and Neutron Powder Diffraction Data. The powder diffraction patterns of $(GeTe)_x(LiSbTe_2)_2$ for x = 0, 1, 2, and 3 could be indexed assuming cubic metrics (cf. Figure 2; enlarged graphs can be found in Figure S1 in the Supporting Information). As Li does not significantly contribute to X-ray diffraction intensities, joint refinements on neutron and X-ray diffraction patterns were performed; lattice parameters, atom coordinates, and displacement parameters were refined simultaneously on both data sets. To refine anisotropic broadening of the reflection profiles of the X-ray data, the LeBail–Jouanneaux algorithm was used.[25] The reflection broadening increases with the GeTe content x. A common displacement factor was refined for all cations and a separate one for Te.

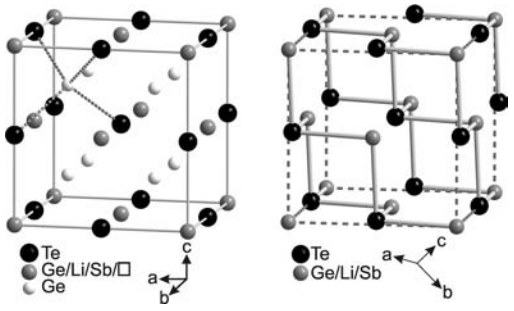

Figure 1. Crystal structure of $(GeTe)_x(LiSbTe_2)_2$: NaCl-type with partially filled tetrahedral voids of fcc packing of Te for x = 2, 3 (left, the occupancy factors of the Ge positions are small, cf. Table 2; the tetrahedral environment is indicated for one of the Ge atoms); GeTe type for x = 6, 11 (right, short interatomic distances are drawn as "bonds", the dotted line corresponds to the unit cell of the related NaCl-type structure, it is not the one of the GeTe type).

dx.doi.org/10.1021/ic401516m | Inorg. Chem. 2013, 52, 11288–11294

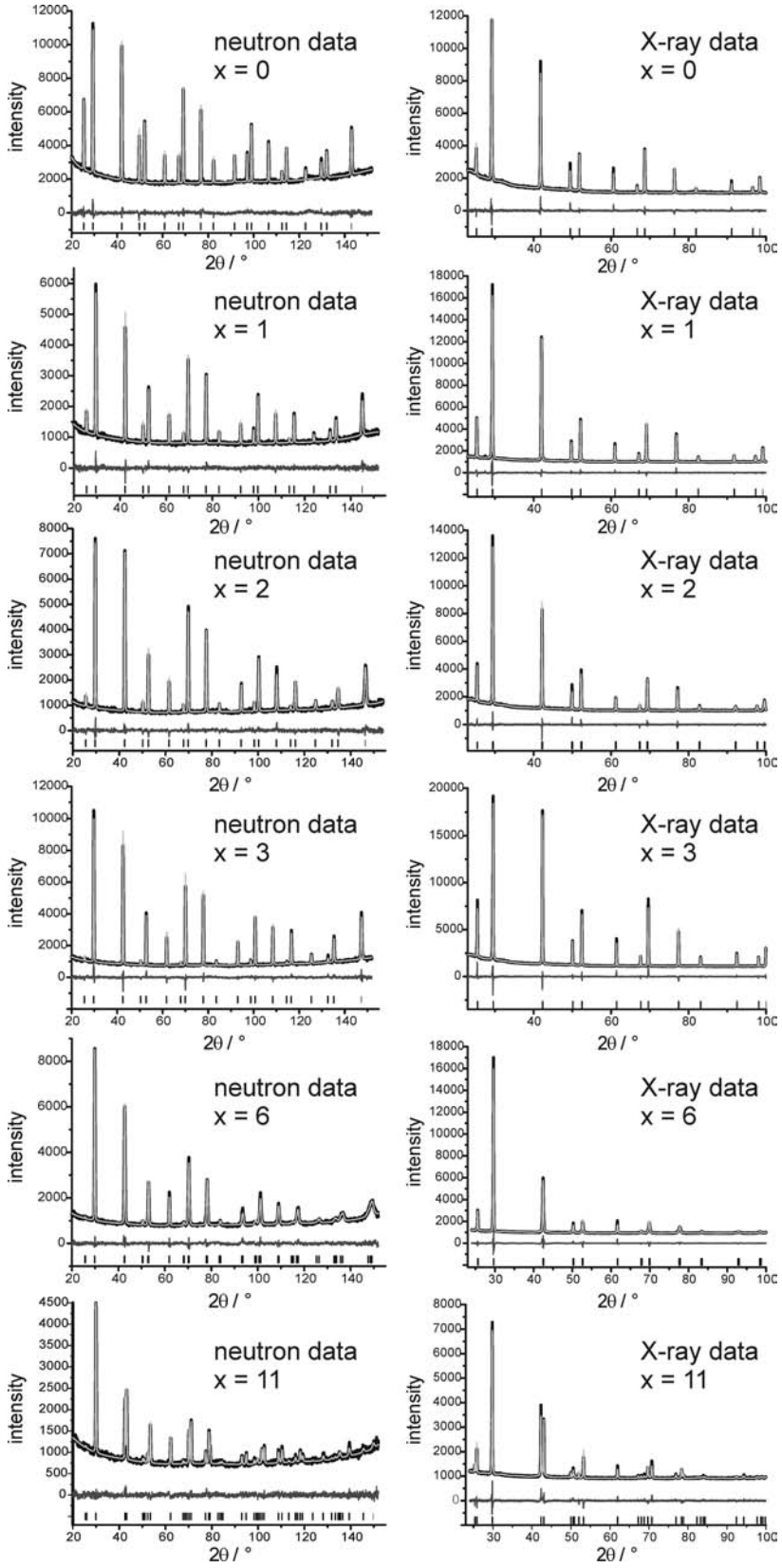

Figure 2. Rietveld fits of the joint refinement of neutron data (left) and X-ray data (right) for $(GeTe)_x(LiSbTe_2)_2$ with x = 0, 1, 2, 3, 6, and 11 (top to bottom): experimental (black) and calculated data (light gray); difference plot (dark gray); peak positions (black, straight lines).

Like $Li_2Sb_2Te_4$ (= $LiSbTe_2$, x = 0),[26] which was prepared for comparison, the average structure of $(GeTe)_x(LiSbTe_2)_2$ for x = 1, 2, and 3 corresponds to a cation-disordered rock-salt-type structure (space group $Fm\bar{3}m$, No. 225). Although profile fits assuming a trigonal setting do not reveal any deviations from cubic metrics, structure models (e.g., the GeTe type)[27,28] with

dx.doi.org/10.1021/ic401516m | *Inorg. Chem.* 2013, 52, 11288−11294

Table 1. Joint Refinement Results of Neutron ($20° \le 2\theta \le 155°$; λ = 1.5484 Å) and X-ray ($23° \le 2\theta \le 100°$; λ = 1.540596 Å, i.e., Cu−Kα_1) Powder Diffraction Data for the $(GeTe)_x(LiSbTe_2)_2$ Phases $Li_2Sb_2Te_4$, $Li_2GeSb_2Te_5$, $Li_2Ge_2Sb_2Te_6$, $Li_2Ge_3Sb_2Te_7$, $Li_2Ge_6Sb_2Te_{10}$, and $Li_2Ge_{11}Sb_2Te_{15}$ Using the Fundamental Parameter Approach

compound	$Li_2Sb_2Te_4$	$Li_2GeSb_2Te_5$	$Li_2Ge_2Sb_2Te_6$	$Li_2Ge_3Sb_2Te_7$	$Li_2Ge_6Sb_2Te_{10}$	$Li_2Ge_{11}Sb_2Te_{15}$
asymmetric unit	$Li_{0.5}Sb_{0.5}Te$	$Li_{0.4}Ge_{0.2}Sb_{0.4}Te$	$Li_{0.33}Ge_{0.33}Sb_{0.33}Te$	$Li_{0.29}Ge_{0.43}Sb_{0.29}Te$	$Li_{0.2}Ge_{0.6}Sb_{0.2}Te$	$Li_{0.13}Ge_{0.73}Sb_{0.13}Te$
GeTe content x	0	1	2	3	6	11
molar mass/g mol^{-1}	191.95	193.6	194.7	195.5	196.9	198.0
Z	4				3	
$F(000)$	316	320	322.4	324.4	246	247.9
crystal system, space group	cubic, $Fm\bar{3}m$ (No. 225)				trigonal, $R3m$ (No. 160)	
lattice parameters/Å	6.10957(3)	6.06904(7)	6.05354(4)	6.03207(6)	a = 4.24590(7) c = 10.4382(2)	a = 4.20290(6) c = 10.5360(2)
volume/Å^3	228.051(3)	223.542(8)	221.834(4)	219.482(7)	162.966(7)	161.178(6)
constraints	1	2	4	4	2	2
number of reflections (neutron)	23	23	23	23	56	54
number of reflections (X-ray)	15	15	15	15	34	31
refined parameters/background	28/48	28/48	29/48	29/48	25/48	25/48
R_p/R_{wp} (neutron)	0.0246/0.0312	0.0325/0.0408	0.0359/0.0454	0.0367/0.0475	0.0341/0.0438	0.0314/0.0396
R_p/R_{wp} (X-ray)	0.0161/0.0246	0.0168/0.0280	0.0165/0.0251	0.0207/0.0359	0.0209/0.0357	0.0170/0.0275
GOF (neutron)	1.327	1.280	1.401	1.516	1.415	1.184
GOF (X-ray)	0.920	0.973	0.886	1.375	1.163	0.876

Table 2. Atom Positions, Site Occupancy Factors (s.o.f.), and Displacement Factors (B_{iso}) for the $(GeTe)_x(LiSbTe_2)_2$ Phases $Li_2Sb_2Te_4$, $Li_2GeSb_2Te_5$, $Li_2Ge_2Sb_2Te_6$, $Li_2Ge_3Sb_2Te_7$, $Li_2Ge_6Sb_2Te_{10}$, and $Li_2Ge_{11}Sb_2Te_{15}$

sum formula	GeTe content x	atom	Wyckoff position	x y z	s.o.f.	B_{iso}
$Li_2Sb_2Te_4$	0	Li, Sb	4*a*	0 0 0	$^1/_2$, $^1/_2$	1.86(2)
		Te	4*b*	$^1/_2$ $^1/_2$ $^1/_2$	1	0.67(2)
$Li_2GeSb_2Te_5$	1	Li, Ge, Sb	4*a*	0 0 0	$^2/_5$, $^1/_5$, $^2/_5$	2.56(1)
		Te	4*b*	$^1/_2$ $^1/_2$ $^1/_2$	1	1.02(1)
$Li_2Ge_2Sb_2Te_6$	2	Li, Ge, Sb	4*a*	0 0 0	$^1/_3$, 0.322(1), $^1/_3$	2.56(2)
		Ge	8*c*	$^1/_4$ $^1/_4$ $^1/_4$	0.0054(6)	= B_{iso}(4*a*)
		Te	4*b*	$^1/_2$ $^1/_2$ $^1/_2$	1	1.36(1)
$Li_2Ge_3Sb_2Te_7$	3	Li, Ge, Sb	4*a*	0 0 0	$^2/_7$, 0.407(1), $^2/_7$	2.28(2)
		Ge	8*c*	$^1/_4$ $^1/_4$ $^1/_4$	0.0104(7)	= B_{iso}(4*a*)
		Te	4*b*	$^1/_2$ $^1/_2$ $^1/_2$	1	1.42(2)
$Li_2Ge_6Sb_2Te_{10}$	6	Li, Ge, Sb	3*a*	0 0 0.4860(4)	$^1/_5$, $^3/_5$, $^1/_5$	2.61(7)
		Te	3*a*	0 0 0	1	1.74(4)
$Li_2Ge_{11}Sb_2Te_{15}$	11	Li, Ge, Sb	3*a*	0 0 0.4817(3)	$^2/_{15}$, $^{11}/_{15}$, $^2/_{15}$	2.17(8)
		Te	3*a*	0 0 0	1	1.72(6)

other reasonable space groups that are typical for GST materials, that is, $R\bar{3}m$ and $R3m$, were considered; however, the refined models showed no deviation from the rock-salt-type structure (e.g., no 3 + 3 instead of octahedral coordination polyhedra). In the rock-salt-type model, all three cations occupy the 4*a* position, while Te occupies the 4*b* anion position. For x = 2 and 3, small positive residual densities were present in the tetrahedral voids (8*c* position), however, only for neutron data (cf. Figure 1, left). Li could be excluded because of its negative neutron scattering length. The strongest neutron scatterer involved is Ge. It was possible to refine an occupancy factor of 0.005 for x = 2 and 0.01 for x = 3 of Ge on the 8*c* position. A sum formula constraint according to the nominal composition confirmed by ICP-OES (cf. Table S1 in the Supporting Information) was used, which means introducing vacancies on the 4*a* position. In addition to its large neutron scattering length, the presence of Ge in part of the tetrahedral voids of fcc packing of Te is corroborated by the fact that, for x = 0, that is, the sample without Ge, no such residual density was observed. For x = 1, the residual density in the tetrahedral void was observed but the refined occupancy is not statistically significant, in contrast to higher Ge contents. Also, note that, in amorphous phases, Ge may also be tetrahedrally coordinated by Te, which was shown for phase-change materials by EXAFS investigations (so-called "umbrella flip").[29] This tetrahedral coordination would imply an sp^3 hybridization of Ge in the amorphous phase, in contrast to its *p*-type configuration in the crystalline GST phases. However, recent investigations show that, whereas, in amorphous phases, most Ge atoms are coordinated octahedrally,[30] some Ge atoms in crystalline phases up may be coordinated tetrahedrally due to Ge-vacancy interactions, for example, in rock-salt-type $Ge_2Sb_2Te_5$.[31] However, ^{125}Te solid-state NMR studies have proven the tetrahedral coordination exclusively in nanocrystalline material.[32] In the cubic Li-doped GST phases discussed in this contribution, the Ge occupation of the tetrahedral void and the

dx.doi.org/10.1021/ic401516m | Inorg. Chem. 2013, 52, 11288−11294

resulting cation vacancies probably lead to local distortions of the atomic structure.

The powder patterns of $(GeTe)_6(LiSbTe_2)_2$ and $(GeTe)_{11}(LiSbTe_2)_2$ could be indexed assuming rhombohedral metrics, which is in accordance with the observed reflection splitting and broadening, respectively (cf. Figure 2; enlarged graphs can be found in Figure S1 in the Supporting Information). Three structure models were taken into account: (a) the CuPt type (space group $R\bar{3}m$, No. 166),[33] which represents a rhombohedrally distorted (along ⟨111⟩) variant of the rock-salt-type structure without layer formation; (b) the GeTe type (space group $R3m$, No. 160),[27] a binary variant of the layered gray As type;[34] and (c) the gray As type itself (space group $R\bar{3}m$, No. 166), which does not allow one to distinguish cations and anions as it has only one crystallographic position. It turned out that both compounds crystallize in a GeTe-type structure (cf. Figure 1, right), because the different scattering densities on cation and anion positions, respectively, are obvious and 3 + 3 coordination of both cations and anions indicates the formation "As-type" layers as the z coordinate of the cations deviates significantly from 0.5. Such deviations from the NaCl type and the metric distortion become more pronounced for increasing GeTe contents x. All cations are disordered on the cation position; Te occupies the anion position. In these trigonal phases, no significant residual scattering densities were observed. Similar to the cubic phases, a common displacement parameter was refined for all cations and a separate one for Te; furthermore, a slight preferred orientation was taken into account using spherical harmonics for the trigonal compounds.

The refined atomic parameters and the details of the structure refinements are given in Tables 1 and 2, respectively. Further details of the crystal structure investigations may be obtained from Fachinformationszentrum Karlsruhe, 76344 Eggenstein-Leopoldshafen, Germany (Fax: (+49)7247-808-666; E-mail: crysdata@fiz-karlsruhe.de, http://www.fiz-karlsruhe.de/request_for_deposited_data.html) on quoting the depository numbers CSD 426293, 426294, 426295, 426296, 426297, and 426298 for x = 0, 1, 2, 3, 6, and 11, respectively.

Temperature-Dependent X-ray Powder Diffraction. As explained in the Introduction, quenched $(GeTe)_nSb_2Te_3$ (GST) compounds with $n > 3$ show a phase transition from the metastable (pseudo)cubic to the trigonal layered phases at ~350 °C and another one to the stable rock-salt-type HT phase at ~450 °C, which is characterized by random disorder of Ge, Sb, and vacancies.[15,35] In contrast to GST, cubic $(GeTe)_x(LiSbTe_2)_2$ compounds (cf. Figure 3, top for x = 2) show no such phase transitions; they are stable between room temperature and the melting point. Because of the exchange of Ge^{2+} with twice the amount of Li^+, no or just very few (for x = 2, 3) cation vacancies remain so that vacancy ordering is not a characteristic structural feature. The full width at half-maximum of the reflections does not change with respect to the temperature; however, the intensities at high angles decrease at higher temperature due to the increasing displacement parameters.

Trigonal $(GeTe)_x(LiSbTe_2)_2$ compounds with $x \geq 6$ (cf. Figure 3, bottom for x = 11) show a phase transition from an average GeTe-type structure to a rock-salt-type cubic high-temperature phase. At temperatures above 280 °C (for x = 11), the coordination number changes from 3 + 3 to 6. This phase transition is similar to that of GeTe itself and has also been observed for TAGS materials $(GeTe)_xAgSbTe_2$.[27,28,36−40] It implies twinning upon cooling the cubic high-temperature

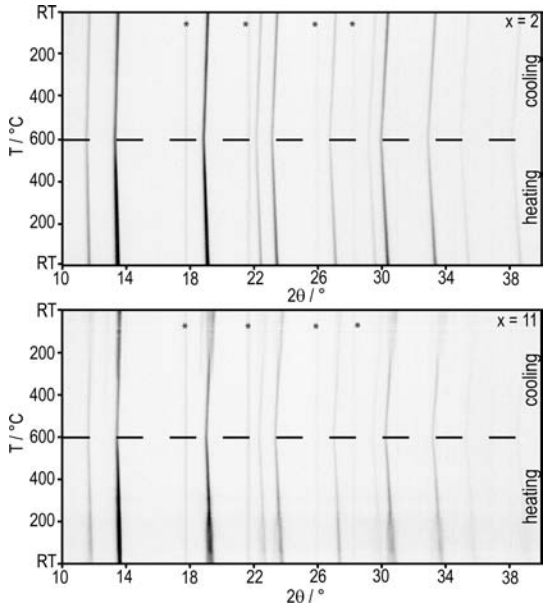

Figure 3. Temperature-dependent powder X-ray diffraction patterns of $(GeTe)_x(LiSbTe_2)_2$ for x = 2 (top) and x = 11 (bottom). The dashed line marks the highest temperature; asterisks (∗) mark the reflections caused by the furnace.

phase due to the *translationengleiche* symmetry reduction from $Fm\bar{3}m$ to $R3m$. The temperature of the phase transition is lower than for $(GeTe)_nSb_2Te_3$, which might be explained by the lack of cation vacancies. The octahedral coordination of Te in $(GeTe)_x(LiSbTe_2)_2$ is impossible for rock-salt-type GST as cation defects, of course, mean incomplete polyhedra around anions. The higher the temperature, the more dominant are entropy effects, which are not required for forming a defect-free rock salt type.

Thermoelectric Properties of $(GeTe)_{11}(LiSbTe_2)_2$. $(GeTe)_{11}(LiSbTe_2)_2$ can be viewed as the Li-substituted variant of metastable $(GeTe)_{12}Sb_2Te_3$; the stoichiometry is also quite similar to that of the well-known thermoelectric material TAGS-85 $(GeTe)_{85}(AgSbTe_2)_{15} = (GeTe)_{11.33}(AgSbTe_2)_2$.[38−40] In contrast to $LiSbTe_2$, which has a band gap of 4.46 eV,[42] the compounds discussed in this section show metallic behavior. The electrical resistivity (ρ) increases with increasing temperature; the absolute values for $(GeTe)_{11}(LiSbTe_2)_2$ are between those of $(GeTe)_{12}Sb_2Te_3$ and TAGS-85 (Figure 4, top). This is probably due to the higher ionicity of the Li-containing compound in comparison to $(GeTe)_{12}Sb_2Te_3$ and a lower charge carrier concentration in comparison to TAGS-85, as indicated by the latter's higher Seebeck coefficient (S). All compounds are p-type conductors as S is positive. In comparison to $(GeTe)_{12}Sb_2Te_3$, S of $(GeTe)_{11}(LiSbTe_2)_2$ is higher at room temperature but does not increase as much as that of $(GeTe)_{12}Sb_2Te_3$ with respect to the temperature, so that it becomes lower at 300 °C (Figure 4, third from top). Both compounds do not reach the extremely high S of TAGS-85; however, they approach it at higher temperatures.

Because of its higher ρ, $(GeTe)_{11}(LiSbTe_2)_2$ exhibits a lower thermal conductivity (κ) than the unsubstituted GST compound (Figure 4, second from top). The phononic contribution to κ is in the same range for both compounds; however, in the low-temperature regime, it is slightly lower for GST, whose crystal structure is characterized by intersecting defect layers. The temperature characteristics of κ reflect the

dx.doi.org/10.1021/ic401516m | Inorg. Chem. 2013, 52, 11288−11294

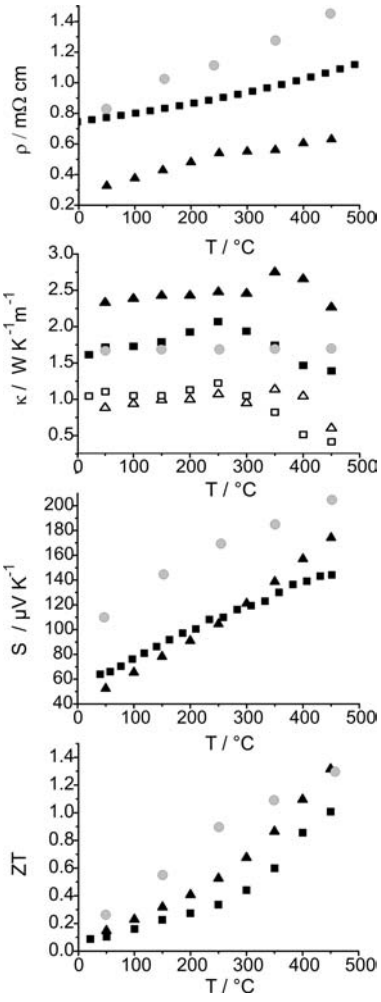

Figure 4. Thermoelectric properties of $(GeTe)_{11}(LiSbTe_2)_2$ (black square) in comparison with $(GeTe)_{12}Sb_2Te_3$ [from ref 15] (black triangle) and $(GeTe)_{11.3}(AgSbTe_2)_2$ [TAGS-85, from ref 41] (gray circle): electrical conductivity (top); total thermal conductivity (second from top) with the phononic part given as empty symbols; Seebeck coefficient (third from top), and the ZT value (bottom).

phase transitions. At ~280 °C, $(GeTe)_{11}(LiSbTe_2)_2$ shows one phase transition before melting; κ increases with respect to the temperature until the rock salt type is formed and then decreases at higher temperatures. Thus, in the 3D rock-salt-type phase, phonon scattering is more effective than in the layered GeTe type, probably because the cation disorder is dynamic up to a certain degree. For $(GeTe)_{12}Sb_2Te_3$, in contrast, κ reflects the two phase transitions described above at 350 and 450 °C, respectively. In this compound, ρ is also affected by the structural changes because the rearrangement of vacancy layers is reconstructive, whereas, for the Li-containing phase, the phase transition just involves slight distortions. In contrast, κ of TAGS-85 is almost constant up to 450 °C. $(GeTe)_{11}(LiSbTe_2)_2$ possesses both a lower κ and a lower ρ and thus a lower phononic contribution of κ than TAGS-85 above 350 °C. This corroborates that Li atoms can be viewed as "pseudo-vacancies". In comparison to $(GeTe)_{12}Sb_2Te_3$, the lower κ of $(GeTe)_{11}(LiSbTe_2)_2$ nearly compensates for the higher ρ. This results in a ZT value of 1.0 at 450 °C (Figure 4, bottom). This is lower than the one of metastable $(GeTe)_{12}Sb_2Te_3$; however, for $(GeTe)_{11}(LiSbTe_2)_2$, it corresponds to a thermodynamically stable phase that does not change its structure upon long-term annealing. The higher ZT value of TAGS-85 is a consequence of its very high S.

4. CONCLUSION

Exchanging Ge^{2+} by twice the amount of Li^+ reduces the concentration of vacancies in $(GeTe)_nSb_2Te_3$ and yields stable compounds of the solid solution series $(GeTe)_x(LiSbTe_2)_2$. These can be viewed as the Li variant of TAGS materials $(GeTe)_xAgSbTe_2$. Li-doped GST elegantly combines the high thermal stability of TAGS with the low phononic contribution to the thermal conductivity of GST compounds, because Li fills the cation vacancies and is very light; which means that it can be viewed as a "pseudo-vacancy". The various defect ordering processes and diffusion phenomena of $(GeTe)_nSb_2Te_3$[15,35] are not observed in $(GeTe)_x(LiSbTe_2)_2$, simply because there are no cation vacancies. Both the average crystal structures and the thermal behavior, that is, the phase transition from the GeTe-type to the rock-salt-type, are comparable to the corresponding features of TAGS materials. However, neutron data for $(GeTe)_x(LiSbTe_2)_2$ (x = 2, 3) indicate that few percent of the Ge atoms occupy the tetrahedral voids, which probably cause distortions of the Te substructure. On the other hand, Li disorder might be dynamic at high temperature. Solid-state NMR might be an intriguing method to further investigate such phenomena.

The thermoelectric properties of $(GeTe)_{11}(LiSbTe_2)_2$ are promising, especially as the compound is long-term stable at all temperatures. The ZT value can probably be further improved by adjusting the GeTe content x and varying the cation vacancy concentration by not completely "filling" all vacancies. Because of the higher ionicity of the Li-doped compounds, the GeTe content of samples with the optimal ZT value is expected to be different from that of GST (n = 12, 19) and TAGS (x = 4, 5.67), respectively.

■ ASSOCIATED CONTENT

Supporting Information

Table containing ICP-OES results and a figure showing enlarged Rietveld fits of the joint refinements of neutron data and X-ray data. This material is available free of charge via the Internet at http://pubs.acs.org.

■ AUTHOR INFORMATION

Corresponding Author

*E-mail: oliver.oeckler@gmx.de. Fax: (+49)341-97-36299.

Notes

The authors declare no competing financial interest.

■ ACKNOWLEDGMENTS

This investigation was funded by the Deutsche Forschungsgemeinschaft (grant OE530/1-2) and the Studienstiftung des deutschen Volkes (fellowship for T.S.). We thank T. Miller for the temperature-dependent powder diffraction experiments and H. Hartl for ICP-OES analyses. We are grateful to Prof. Dr. W. Schnick for his generous support of this work.

■ REFERENCES

(1) Wuttig, M.; Raoux, S. *Z. Anorg. Allg. Chem.* **2012**, *638*, 2455.
(2) Siegrist, T.; Merkelbach, P.; Wuttig, M. *Annu. Rev. Condens. Matter Phys.* **2012**, *3*, 215.
(3) Raoux, S. *Annu. Rev. Mater. Res.* **2009**, *39*, 9.

(4) Matsunaga, T.; Morita, H.; Kojima, R.; Yamada, N.; Kifune, K.; Kubota, Y.; Tabata, Y.; Kim, J.-J.; Kobata, M.; Ikenaga, E.; Kobayashi, K. *J. Appl. Phys.* **2008**, *103*, 093511.
(5) Konstantinov, P. P.; Shelimova, L. E.; Avilov, E. S.; Kretova, M. A.; Zemskov, V. S. *Inorg. Mater.* **2001**, *37*, 788.
(6) Shelimova, L. E.; Karpinskii, O. G.; Kretova, M. A.; Kosyakov, V. I.; Shestakov, V. A.; Zemskov, V. S.; Kuznetsov, F. A. *Inorg. Mater.* **2000**, *36*, 928.
(7) Shelimova, L. E.; Karpinskii, O. G.; Konstantinov, P. P.; Kretova, M. A.; Avilov, E. S.; Zemskov, V. S. *Inorg. Mater.* **2001**, *37*, 421.
(8) Schneider, M. N.; Rosenthal, T.; Stiewe, C.; Oeckler, O. *Z. Kristallogr.* **2010**, *225*, 463.
(9) Matsunaga, T.; Yamada, N.; Kubota, Y. *Acta Crystallogr., Sect. B* **2004**, *60*, 685.
(10) Wuttig, M.; Yamada, N. *Nat. Mater.* **2007**, *6*, 824.
(11) Wuttig, M.; Luesebrink, D.; Wamwangi, D.; Welnic, W.; Gillessen, M.; Dronskowski, R. *Nat. Mater.* **2007**, *6*, 122.
(12) Wuttig, M. *Phys. Status Solidi B* **2012**, *249*, 1843.
(13) Zhang, W.; Thiess, A.; Zalden, P.; Zeller, R.; Dederichs, P. H.; Raty, J.-Y.; Wuttig, M.; Blügel, S.; Mazzarello, R. *Nat. Mater.* **2012**, *11*, 952.
(14) Waser, R.; Dittmann, R.; Salinga, M.; Wuttig, M. *Int. J. Mater. Res.* **2010**, *101*, 182.
(15) Rosenthal, T.; Schneider, M. N.; Stiewe, C.; Döblinger, M.; Oeckler, O. *Chem. Mater.* **2011**, *23*, 4349.
(16) Medlin, D. L.; Snyder, G. J. *Curr. Opin. Colloid Interface Sci.* **2009**, *14*, 226.
(17) Kanatzidis, M. G. *Chem. Mater.* **2010**, *22*, 648.
(18) Lan, Y. C.; Minnich, A. J.; Chen, G.; Ren, Z. F. *Adv. Funct. Mater.* **2010**, *20*, 357.
(19) Sootsman, J. R.; Chung, D. Y.; Kanatzidis, M. G. *Angew. Chem., Int. Ed.* **2009**, *48*, 8616.
(20) Sittner, E.-R.; Siegert, K. S.; Jost, P.; Schlockermann, C.; Lange, F. R. L.; Wuttig, M. *Phys Status Solidi A* **2013**, *1*, 147.
(21) Zhang, S. N.; Zhu, T. J.; Yang, S. H.; Yu, C.; Zhao, X. B. *Acta Mater.* **2010**, *58*, 4160.
(22) *TOPAS-Academic*, V. 4.1; Coelho Software: Brisbane, Australia, 2007.
(23) de Boor, J.; Stiewe, C.; Ziolkowski, P.; Dasgupta, T.; Karpinski, G.; Lenz, E.; Edler, F.; Müller, E. *J. Electron. Mater.* **2013**, *42*, 1711.
(24) de Boor, J.; Müller, E. *Rev. Sci. Instrum.* **2013**, *84*, 065102.
(25) LeBail, A.; Jouanneaux, A. *J. Appl. Crystallogr.* **1997**, *30*, 265.
(26) Evain, M.; Boucher, F.; Brec, R.; Rouxel, J.; Jung, J. S.; O'Connor, C. J. *Eur. J. Solid State Inorg. Chem.* **1992**, *29*, 1055.
(27) Klemm, W.; Frischmuth, G. *Z. Anorg. Allg. Chem.* **1934**, *218*, 249.
(28) Chattopadhyay, T.; Boucherle, J. X.; vonSchnering, H. G. *J. Phys. C: Solid State Phys.* **1987**, *20*, 1431.
(29) Kolobov, A. V.; Fons, P.; Frenkel, A. I.; Ankudinov, A. L.; Tominaga, J.; Uruga, T. *Nat. Mater.* **2004**, *3*, 703.
(30) Xu, M.; Cheng, Y. Q.; Sheng, H. W.; Ma, E. *Phys. Rev. Lett.* **2009**, *103*, 195502.
(31) Liu, X. Q.; Li, X. B.; Zhang, L.; Cheng, Y. Q.; Yan, Z. G.; Xu, M.; Han, X. D.; Zhang, S. B.; Zhang, Z.; Ma, E. *Phys. Rev. Lett.* **2011**, *106*, 025501.
(32) Sen, S.; Edwards, T. G.; Cho, J.-Y.; Joo, Y.-C. *Phys. Rev. Lett.* **2012**, *108*, 195506.
(33) Johannson, C. H.; Linde, J. O. *Ann. Phys. (Leipzig, Ger.)* **1927**, *82*, 449.
(34) Bradley, A. J. *Philos. Mag.* **1924**, *47*, 657.
(35) Schneider, M. N.; Biquard, X.; Stiewe, C.; Schröder, T.; Urban, P.; Oeckler, O. *Chem. Commun.* **2012**, *48*, 2192.
(36) Goldak, J.; Barrett, C. S.; Innes, D.; Youdelis, W. *J. Chem. Phys.* **1966**, *44*, 3323.
(37) Fons, P.; Kolobov, A. V.; Krbal, M.; Tominaga, J.; Andrikopoulos, K. S.; Yannopoulos, S. N.; Voyiatzis, G. A.; Uruga, T. *Phys. Rev. B* **2010**, *82*, 155209.
(38) Cook, B. A.; Kramer, M. J.; Wei, X.; Harringa, J. L.; Levin, E. M. *J. Appl. Phys.* **2007**, *101*, 053715.
(39) Wood, C. *Rep. Prog. Phys.* **1988**, *51*, 459.
(40) Rosi, F. D.; Dismukes, J. P.; Hockings, E. F. *Electron. Eng.* **1960**, *79*, 450.
(41) Davidow, J.; Gelbstein, Y. *J. Electron. Mater.* **2013**, *42*, 1542.
(42) Kang, S.-G.; Chae, W.-S.; Kim, Y.-R.; Jung, J.-S.; Lee, S.-H. *Chem. Phys.* **2000**, *256*, 295.